Earth and Planetary Science Letters 369–370 (2013) 108–119

Contents lists available at SciVerse ScienceDirect

Earth and Planetary Science Letters

journal homepage: www.elsevier.com/locate/epsl

Diurnal to interannual rainfall $\delta^{18}O$ variations in northern Borneo driven by regional hydrology

Jessica W. Moerman [a,*], Kim M. Cobb [a], Jess F. Adkins [b], Harald Sodemann [c], Brian Clark [d], Andrew A. Tuen [e]

[a] School of Earth and Atmospheric Sciences, Georgia Institute of Technology, 311 Ferst Drive, Atlanta, GA 30332, United States
[b] Division of Geological and Planetary Sciences, California Institute of Technology, 1200 E. California Blvd., Pasadena, CA 91125, United States
[c] Institute for Atmospheric and Climate Science, ETH Zürich, Universitätstrasse 16, 8092 Zürich, Switzerland
[d] Gunung Mulu National Park, Sarawak, Malaysia
[e] Institute of Biodiversity and Environmental Conservation, Universiti Malaysia Sarawak, 94300 Kota Samarahan, Malaysia

ARTICLE INFO

Article history:
Received 4 October 2012
Received in revised form
11 March 2013
Accepted 13 March 2013
Editor: G. Henderson
Available online 25 April 2013

Keywords:
rainfall oxygen isotopes
Madden–Julian oscillation
amount effect
stalagmite
paleoclimate
El Niño southern oscillation

ABSTRACT

The relationship between climate variability and rainfall oxygen isotopic ($\delta^{18}O$) variability is poorly constrained, especially in the tropics, where many key paleoclimate records rely on past rainfall isotopes as proxies for hydroclimate. Here we present a daily-resolved, 5-yr-long timeseries of rainfall $\delta^{18}O$ from Gunung Mulu National Park, located in northern Borneo (4°N, 114°E) in the heart of the West Pacific Warm Pool, and compare it to local and regional climatic variables. Daily rainfall $\delta^{18}O$ values range from +0.7‰ to −18.5‰ and exhibit a weak but significant inverse relationship with daily local precipitation amount ($R=-0.19$, $p<0.05$), consistent with the tropical amount effect. Day-to-day $\delta^{18}O$ variability at Mulu is best correlated to regional precipitation amount averaged over the preceding week ($R=-0.64$, $p<0.01$). The inverse relationship between Mulu rainfall $\delta^{18}O$ and local (regional) precipitation amount increases with increased temporal averaging, reaching $R=-0.56$ ($R=-0.72$) on monthly timescales. Large, negative, multi-day rainfall $\delta^{18}O$ anomalies of up to 16‰ occur every 30–90 days and are closely associated with wet phases of the intraseasonal Madden–Julian Oscillation. A weak, semi-annual seasonal cycle in rainfall $\delta^{18}O$ of 2–3‰ bears little resemblance to seasonal precipitation variability, pointing to a complex sequence of moisture sources and/or trajectories over the course of the year. Interannual rainfall $\delta^{18}O$ variations of 6–8‰ are significantly correlated with indices of the El Niño Southern Oscillation, with increased rainfall $\delta^{18}O$ during relatively dry El Niño conditions, and vice versa during La Nina events. We find that Mulu rainfall $\delta^{18}O$ outperforms Mulu precipitation amount as a tracer of basin-scale climate variability, highlighting the time- and space-integrative nature of rainfall $\delta^{18}O$. Taken together, our results suggest that rainfall $\delta^{18}O$ variability at Mulu is significantly influenced by the strength of regional convective activity. As such, our study provides further empirical support for the interpretation of $\delta^{18}O$-based paleo-reconstructions from northern Borneo stalagmites as robust indicators of regional-scale hydroclimate variability, where higher $\delta^{18}O$ reflects regional drying.

1. Introduction

The inverse relationship between tropical precipitation amount and rainfall isotopic values, known as the 'amount effect' (Dansgaard, 1964; Rozanski et al., 1993; Araguas-Araguas et al., 1998), has provided the basis for numerous reconstructions of tropical paleohydrology from lake deposits (e.g. Sachs et al., 2009; Tierney et al., 2010), alpine ice cores (e.g. Hoffmann et al., 2003; Vimeux et al., 2009) and stalagmite calcite (e.g. Bar-Matthews et al., 1997; Burns et al., 1998; Wang et al., 2001). Such reconstructions play a key role in resolving past tropical climate changes, as continuous, high-resolution paleoclimate archives are relatively rare in the tropics. Stalagmite $\delta^{18}O$ records, in particular, have been used to probe hydroclimate variability over the last hundred years (Treble et al., 2005; Frappier et al., 2007), the last glacial cycle (Dykoski et al., 2005; Partin et al., 2007; Griffiths et al., 2009), and the last million years (Wang et al., 2001; Meckler et al., 2012).

Despite robust observations of the amount effect across tropical latitudes, the climatic controls on rainfall $\delta^{18}O$ at any given site remain highly uncertain as numerous processes contribute to rainfall $\delta^{18}O$ variability. Rayleigh distillation, whereby cumulative fractionation during condensation and rainout leaves the residual

* Corresponding author. Tel.: +1 404 894 3893; fax: +1 404 894 5638.
E-mail addresses: jessica.moerman@gatech.edu (J.W. Moerman), kcobb@eas.gatech.edu (K.M. Cobb), jess@gps.caltech.edu (J.F. Adkins), harald.sodemann@env.ethz.ch (H. Sodemann), brianclark@mulupark.com (B. Clark), aatuen@ibec.unimas.my (A.A. Tuen).

0012-821X/$ - see front matter © 2013 Elsevier B.V. All rights reserved.
http://dx.doi.org/10.1016/j.epsl.2013.03.014

atmospheric vapor depleted in $\delta^{18}O$, has long been recognized as a first-order mechanism driving the amount effect and rainfall $\delta^{18}O$ variability (Dansgaard, 1964; Rozanski et al., 1993). The Rayleigh mechanism operates both locally, in the case of rainfall $\delta^{18}O$ fractionation across a single rainfall event (e.g. Celle-Jeanton et al., 2004) and regionally, when considering the progressive vapor depletion of air parcels transiting through a region of enhanced precipitation (e.g. Cobb et al., 2007; Vimeux et al., 2011).

Several post-condensation processes also likely contribute to the observed amount effect relationship. For one, the evaporation of falling raindrops causes the residual rainfall to be relatively enriched—a process that is maximized in arid regions and during dry seasons (Dansgaard, 1964; Stewart, 1975; Gat, 1996; Lee and Fung, 2008; Risi et al., 2008a). In regions characterized by strong convection, the recycling of water vapor within the convective cell drives rainfall $\delta^{18}O$ lower during episodes of intense convection (Lawrence and Gedzelman, 1996; Lawrence et al., 2004; Risi et al., 2008a, 2008b). Numerous studies have identified additional processes, such as atmospheric mixing and/or changes in moisture sources and trajectories, that contribute to rainfall $\delta^{18}O$ variability at tropical and subtropical sites (Aggarwal et al., 2004; Cobb et al., 2007; Tian et al., 2007; Breitenbach et al., 2010, Gao et al., 2011).

Previous studies have referred to the amount effect in describing fractionation processes that act strictly locally (e.g. Vuille et al., 2005; Lee et al., 2009; LeGrande and Schmidt, 2009) as well as fractionation processes that integrate across larger spatial scales and longer time periods (e.g. Cobb et al., 2007; Risi et al., 2008b; Kurita et al., 2009, 2011; Tremoy et al., 2012). For the sake of clarity, we will differentiate between a "local" versus "regional" amount effect in our study, based on the inferred spatial scale of the fractionation mechanism in question.

Isotope-equipped general circulation models (GCMs) allow for the systematic investigation of the various dynamics regulating rainfall isotopic composition (Joussaume et al., 1984; Jouzel et al., 1987; Hoffmann et al., 1998; Noone and Simmonds, 2002; Schmidt et al., 2007; Tindall et al., 2009; Risi et al., 2010). Agreement between observations and model output has improved as models incorporate processes such as post-condensation raindrop re-evaporation and convective mixing (Field et al., 2010) and as higher spatial resolution affords more realistic model topographies and better representations of weather systems (Vimeux et al., 2011; Gao et al., 2011). Recent studies using isotope-equipped GCMs find that the dominant drivers of rainfall isotopic variability vary from region to region (Lee et al., 2007; Lewis et al., 2010; Conroy et al., in press), with modeled $\delta^{18}O$ values reflecting the net sum of often competing processes (Field et al., 2010). Models also reveal that the relationship between climate and rainfall $\delta^{18}O$ at a given site may vary with time period (e.g. LeGrande and Schmidt, 2009).

The dearth of high-resolution rainfall $\delta^{18}O$ isotope timeseries throughout the tropics makes it difficult to assess the accuracy of fractionation mechanisms that emerge in isotope-equipped model simulations. Most rainfall $\delta^{18}O$ studies rely on the International Atomic Energy Agency–Global Network of Isotopes in Precipitation database (IAEA–GNIP; International Atomic Energy Agency, 2006). As this network is comprised almost exclusively of monthly averaged rainfall $\delta^{18}O$ data, such studies are limited to investigating seasonal and longer timescales. As a result, relatively little is known about rainfall $\delta^{18}O$ variability on daily to intraseasonal (30–90 day) timescales and its connection to dominant intraseasonal climate modes, such as the Madden–Julian Oscillation (MJO; Madden and Julian, 1972; Zhang, 2005). Furthermore, the relatively sparse spatial coverage of the GNIP database in the deep tropics means that the relationship between interannual rainfall $\delta^{18}O$ variability and the El Niño Southern Oscillation (ENSO) is poorly constrained. Additional rainfall isotope timeseries from the tropics help to constrain the modern-day dynamical controls on rainfall $\delta^{18}O$ variability in the tropics, while providing much-needed interpretive frameworks for tropical rainfall $\delta^{18}O$ paleo-reconstructions.

Here we present a 5-yr quasi-continuous collection of cumulative daily rainfall $\delta^{18}O$ from Gunung Mulu National Park (4°N, 114°E), located in northwestern Borneo, in the heart of the West Pacific Warm Pool (WPWP). We investigate the variability of northern Borneo rainfall $\delta^{18}O$ and its response to local and regional climate variations on synoptic to interannual timescales. We also investigate the evolution of rainfall $\delta^{18}O$ across a single rainfall event in order to constrain the sub-diurnal influences on rainfall $\delta^{18}O$ at our site. By comparing these rainfall $\delta^{18}O$ timeseries to local and regional climate variables as well as to indices of large-scale climate variability, we investigate the relationship of rainfall $\delta^{18}O$ in northern Borneo to both local and large-scale climate controls across a range of timescales. We also briefly present rainfall δD data from Gunung Mulu in to order to plot meteoric water lines and compute values of deuterium-excess, a parameter derived from $\delta^{18}O$ and δD (deuterium-excess $= \delta D - 8 \times \delta^{18}O$ (Dansgaard, 1964)) and hereafter referred to as 'd-excess.' There is no GNIP station on Borneo, so our study represents an important addition to the rainfall $\delta^{18}O$ data archive, while informing the climatic interpretation of numerous stalagmite $\delta^{18}O$-based paleoclimate records from our site (Partin et al., 2007; Meckler et al., 2012; Carolin et al., under review).

2. Methods

2.1. Site description

Gunung Mulu National Park receives over 5 m of precipitation annually, which exhibits significant intraseasonal (30–90 days) and interannual variability. The vast majority of this precipitation is delivered by discrete convective events that typically occur in the afternoon. Since northern Borneo lies within the migration path of the Intertropical Convergence Zone (ITCZ) year-round, seasonal variations in precipitation at Mulu are weak. As a result, the climate of northern Borneo is primarily controlled by intraseasonal and interannual precipitation variability associated with the MJO and ENSO respectively, with strong ENSO phases producing annual precipitation anomalies of up to $\pm 50\%$ (Bell and Halpert, 1998). During El Nino events, anomalously warm sea surface temperatures (SST) in the eastern and central tropical Pacific pull the center of deep atmospheric convection east of the Maritime continent (Rasmusson and Wallace, 1983), decreasing convection across the WPWP (Fig. S1). Conversely, convective activity in the WPWP increases during La Niña events. Comprehensive descriptions of the climatic and geologic setting of Gunung Mulu National Park are presented in Cobb et al. (2007).

2.2. Rainfall $\delta^{18}O$ sampling procedure and analysis

Two distinct rainfall sampling campaigns were conducted for this study: (1) a daily collection of rainfall $\delta^{18}O$ at the Gunung Mulu airport from July 2006 to May 2011, and (2) a high-resolution sampling of an individual precipitation event at a remote field camp at Gunung Mulu on March 7, 2010. For the daily rainfall $\delta^{18}O$ collection ($N = 1203$), rainfall was collected in a splayed-bottom rain gauge (Casella model M114003; 254 mm diameter; ~1 m above ground level) at the Mulu Meteorological Station headquartered at Mulu Airport (4.05°N, 114.81°E) and transferred to glass vials, leaving no headspace when precipitation amounts allowed, each morning at 8:00AM MYT. Precipitation amounts were logged at the same time—we refer to this timeseries as 'local Mulu precipitation' hereafter. Rainfall aliquots collected between

July 2006 and February 2010 were stored in 4 mL glass vials with polyseal screw caps and sealed with parafilm. Aliquots collected from March 2010 onwards were stored in 3 mL glass serum vials and sealed with rubber stoppers and crimped aluminum closures, which provided a superior seal than the screw caps.

The use of an open-air rain gauge raises the possibility of isotopic enrichment of the rainfall samples by evaporation over the course of the day. To assess the impact of evaporative enrichment on rainfall isotopic values and to develop guidelines for identifying potentially affected samples, several quality control assessments were performed (see Supplemental Section for details). Based on the findings of these assessments, rainfall samples associated with precipitation amounts less than 1.6 mm were excluded from the final dataset. Evaporation within a vial with headspace represents another source of post-deposition enrichment. As a result, samples stored in vials that were less than 4/5 full were also excluded from the final dataset. Together, this resulted in the exclusion of 176 samples. An additional 23 samples collected in December 2006 were excluded due to documented sampling errors by Mulu personnel. In total, 199 rainfall $\delta^{18}O$ samples were excluded from the final dataset tally ($N=1004$). The exclusion of these samples did not significantly alter the variability of the 5-yr timeseries (Fig. S5).

We also conducted detailed rainfall sampling across a single precipitation event on March 7, 2010 at Camp 5 (4.14°N, 114.89°E), located approximately 12 km NE of Gunung Mulu National Park headquarters. Rainfall $\delta^{18}O$ samples were collected manually at one to four minute intervals (depending on rainfall intensity) throughout the event, for a total of 19 samples. The event lasted for approximately one hour, including a 20-min break in rainfall. Lacking any way to quantitatively measure rainfall rates at the remote field camp, we recorded relative rainfall intensity at the time of each sample collection, where '1' represented a light drizzle and '10' represented the heaviest of downpours. Samples were stored in 3 mL glass serum vials sealed with rubber stoppers and crimped aluminum closures.

Rainfall $\delta^{18}O$ and δD were measured at the Georgia Institute of Technology via cavity ring-down spectroscopy (Picarro L1102-i water isotope analyzer). To calibrate the isotopic composition of the rainfall samples, three internal water standards, each calibrated against NIST-VSMOW, NIST-GISP, and NIST-SLAP, were analyzed at the beginning and end of each analysis. An internal water standard was analyzed after every nine rainfall samples to monitor instrument drift. Memory corrections were applied to each measurement based on empirical, instrument-specific memory coefficients. The long-term reproducibility of this technique is better than $\pm 0.1‰$ for $\delta^{18}O$ and $\pm 0.8‰$ for δD (1σ). In the case of the screw-top vials, sampling and storage contributed an additional uncertainty of $\pm 0.1‰$ (1σ) for $\delta^{18}O$ and $\pm 0.7‰$ (1σ) for δD, as determined by measuring 34 pairs of duplicate rainfall samples. Crimp-top vial duplicates provided indistinguishable $\delta^{18}O$ and δD values. As such, a conservative estimate of uncertainty of $\pm 0.2‰$ (1σ) is attributed to each rainfall $\delta^{18}O$ measurement and $\pm 1.5‰$ (1σ) to each δD measurement. We report an uncertainty of $\pm 1.5‰$ for d-excess values, calculated from the quadratic combination of the uncertainties for $\delta^{18}O$ and δD.

2.3. Gridded climate datasets

We use daily and monthly values of both the Tropical Rainfall Measuring Mission (TRMM 3B42 V6 and 3B43 V6 respectively; $0.25^\circ \times 0.25^\circ$) precipitation data (Huffman et al., 2007) and NOAA Interpolated Outgoing Longwave Radiation dataset (OLR; $2.5^\circ \times 2.5^\circ$; Liebmann and Smith, 1996) to investigate regional convective activity, following Arkin and Ardanuy (1989). SST-derived indices of ENSO variability (i.e. NIÑO3, NIÑO3.4, and NIÑO4) are derived from monthly NOAA Optimum Interpolation Sea Surface Temperature (OISST V2; Reynolds et al., 2002). The significance of correlations between Mulu rainfall $\delta^{18}O$, local Mulu precipitation amount, and the gridded climate datasets listed above is assessed via the Student's *t*-test using effective degrees of freedom, following Bretherton et al. (1999).

3. Results

3.1. Rainfall isotope timeseries across a single convective event

The timeseries of rainfall $\delta^{18}O$ and d-excess across the March 7, 2010 rainfall event are shown in Fig. 1A. Over a 1-h period, rainfall $\delta^{18}O$ ranges from $-1.5‰$ to $+0.8‰$, and δD ranges from $+1.8‰$ to $+10‰$ (not shown), with the highest isotopic values observed in the first minutes of the event. Rainfall isotope values reach their lowest values after fifteen minutes and then gradually increase thereafter, following a "V-shaped" progression documented at higher latitude sites (Rindsberger et al., 1990; Celle-Jeanton et al., 2004).

Fig. 1B illustrates the strong inverse relationship between rainfall $\delta^{18}O$ and relative rainfall intensity ($R=-0.82$) across the March 7th precipitation event, consistent with the amount effect. The strong correlations between d-excess, which is an indicator of

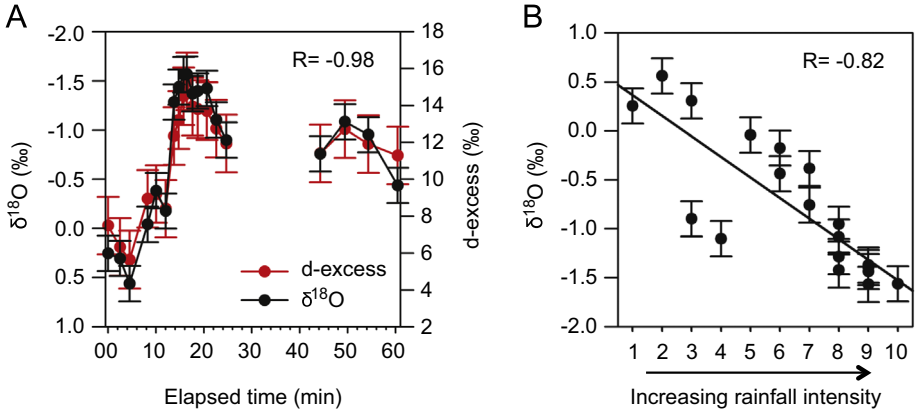

Fig. 1. (A) Mulu rainfall $\delta^{18}O$ (black circles) and d-excess (red circles) during the March 7, 2010 convective event, plotted with error bars of $\pm 0.2‰$ (1σ) for Mulu rainfall $\delta^{18}O$ and $\pm 1.5‰$ (1σ) for d-excess. Note that axes for $\delta^{18}O$ and d-excess are inverted. (B) Relationship between rainfall $\delta^{18}O$ and relative precipitation intensity during the March 7th convective event, where '1' represents a light drizzle and '10' represents the most intense downpour based on qualitative assessment of relative precipitation intensities. Error bars represent $\pm 0.2‰$ (1σ). (For interpretation of the references to color in this figure legend, the reader is referred to the web version of this article.)

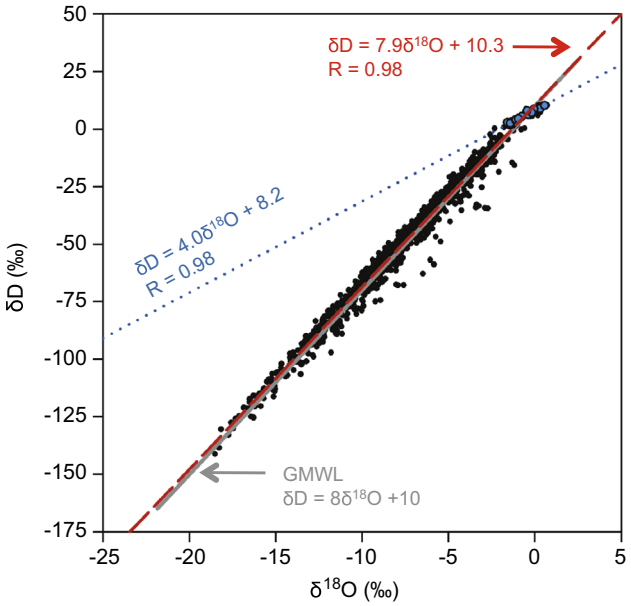

Fig. 2. Mulu rainfall $\delta^{18}O$ versus δD for the daily 5-yr timeseries (black circles) and the March 7, 2010 convective event (blue circles). The dashed red line represents a linear fit for the 5-yr timeseries of daily Mulu rainfall samples. The dotted blue line represents a linear fit for the March 7, 2010 event samples. The global meteoric water line (solid gray line) is plotted for reference (Craig, 1961). (For interpretation of the references to color in this figure legend, the reader is referred to the web version of this article.)

kinetic fractionation (Dansgaard, 1964; Gat, 1996; Risi et al., 2010), and both rainfall $\delta^{18}O$ ($R=-0.98$) and rainfall intensity ($R=0.80$) suggest that the partial re-evaporation of falling raindrops likely drives the amount effect during this event. When raindrops undergo evaporation in low relative humidity conditions, the d-excess value of the evaporate increases, leaving the raindrops with lower d-excess, as seen mostly in the beginning of the March 7th event (Fig. 1A). Further support for post-condensation evaporation is provided by the relatively low slope (~4) for rainfall δD vs. $\delta^{18}O$ variations for this event (Fig. 2), which is typical of evaporation and differs appreciably from the equilibrium $\delta D/\delta^{18}O$ slope of 8 associated with the global meteoric water line (GMWL; Dansgaard, 1964). These data support a central role for post-condensation evaporation during the March 7th convective event, whereby a raindrop is isotopically enriched during its transit from cloud to ground. Such a mechanism also explains the occurrence of several positive rainfall $\delta^{18}O$ values during this event. Together, these results strongly suggest that post-condensation evaporative processes drive the observed "local" amount effect, and rainfall $\delta^{18}O$ variability in general, during this convective event. Our results provide further observational support for recent studies of an idealized microphysical model (Lee and Fung, 2008) and a single column model (Risi et al., 2008a), which both suggest that post-condensation evaporation is an important contributor to the amount effect within individual rainfall events. Additional high-resolution sampling of water isotopes across discrete convective events is needed, however, to confirm whether these results are representative of precipitation events at our site.

3.2. Multi-year timeseries of daily rainfall $\delta^{18}O$

Daily rainfall $\delta^{18}O$ values vary considerably throughout the 5-yr timeseries, ranging from +0.7‰ to −18.5‰ (Fig. 3). Daily rainfall $\delta^{18}O$ values average -7.8 ± 3.6‰ (1σ, $N=1004$), and δD values average -51.7 ± 28.9‰ (1σ, $N=1004$, not shown). The precipitation amount-weighted $\delta^{18}O$ timeseries is nearly identical to the raw $\delta^{18}O$ timeseries (Fig. S5), except that its mean $\delta^{18}O$ value is shifted lower by roughly −0.5‰ because higher precipitation days are also, on average, lower rainfall $\delta^{18}O$ days. Several daily rainfall $\delta^{18}O$ values fall to the right of the local meteoric water line (LMWL; Fig. 2), providing evidence for a role, albeit limited, of evaporative forcing on daily rainfall $\delta^{18}O$ at the site (Dansgaard, 1964). Overall, however, the Mulu LMWL is indistinguishable from the GMWL, indicating that local post-condensation evaporation has minimal impact on cumulative daily rainfall $\delta^{18}O$ (Fig. 2). This finding is further supported by a near-zero correlation between daily rainfall $\delta^{18}O$ and d-excess ($R=-0.01$).

3.2.1. The amount effect at daily and longer timescales

As shown in Fig. 4A, the inverse correlation between daily rainfall $\delta^{18}O$ and daily precipitation amount at Mulu is significant but relatively weak ($R=-0.19$, $p<0.05$). Correlations between rainfall $\delta^{18}O$ and local Mulu precipitation amount are higher on monthly timescales ($R=-0.56$, $p<0.01$; Fig. 4B). Indeed, Fig. 4C further illustrates that the correlation between rainfall $\delta^{18}O$ and Mulu precipitation increases with increased temporal averaging. Correlations with Mulu rainfall $\delta^{18}O$ are even higher for TRMM precipitation and OLR integrated across a $2.5^\circ \times 2.5^\circ$ gridbox centered at 5°N, 115°E containing Gunung Mulu, indicating that regional convective activity explains a larger fraction of Mulu rainfall $\delta^{18}O$ variability at daily and longer timescales than local precipitation. Basin-wide correlations between daily Mulu rainfall $\delta^{18}O$ and gridded TRMM precipitation amount further demonstrate that daily variations in Mulu rainfall $\delta^{18}O$ are closely tied to regional-scale processes (Fig. 5A). This spatial map can be contrasted to the map of correlations between Mulu precipitation amount and gridded TRMM precipitation amount, in which high correlations are confined to the immediate vicinity of the site (Fig. 5B).

While daily Mulu rainfall $\delta^{18}O$ variations are weakly correlated to daily Mulu precipitation amount, they are highly correlated to Mulu precipitation averaged over the previous 8 days ($R=-0.46$; Fig. 4D). Similar results are found using TRMM precipitation and OLR but with correlations peaking with ~5 days of averaging (Fig. 4D). This result reflects the time-integrative nature of rainfall $\delta^{18}O$ that previous studies have observed (Risi et al., 2008b; Vimeux et al., 2011) and modeled (Sturm et al., 2007; Risi et al., 2008a). It should be noted that a simple 8-day lag of local Mulu precipitation (as opposed to an 8-day integration of Mulu precipitation) is not correlated to daily Mulu rainfall $\delta^{18}O$ values ($R=-0.07$), indicating that a simple lag relationship is not responsible for these observations. The time-integrative nature of Mulu rainfall $\delta^{18}O$ is also illustrated by high auto-correlation of the $\delta^{18}O$ timeseries ($R_{AC}=0.45$) compared with that for local Mulu precipitation ($R_{AC}=0.23$). We hypothesize that the week-long 'memory' of rainfall $\delta^{18}O$ may reflect an approximately week-long atmospheric residence time of water vapor at Mulu.

3.2.2. Intraseasonal variability of rainfall $\delta^{18}O$

The daily rainfall $\delta^{18}O$ timeseries is characterized by several exceptionally large (~10‰) negative excursions that occur every 30–90 days and last for several days to one week (Fig. 3). In order to characterize the evolution of these dramatic excursions and investigate their dynamical origins, we isolated eighteen of the largest excursions, hereafter referred to as 'depletion events', by applying a statistical filter that selected excursions based on their amplitude and abruptness (Table S1; see Supplemental Section for selection criteria). The resulting 'depletion events' are marked by triangles along the upper x-axis of Fig. 3.

A composite of the eighteen rainfall $\delta^{18}O$ 'depletion events' reveals consistent relationships between rainfall $\delta^{18}O$, local Mulu precipitation

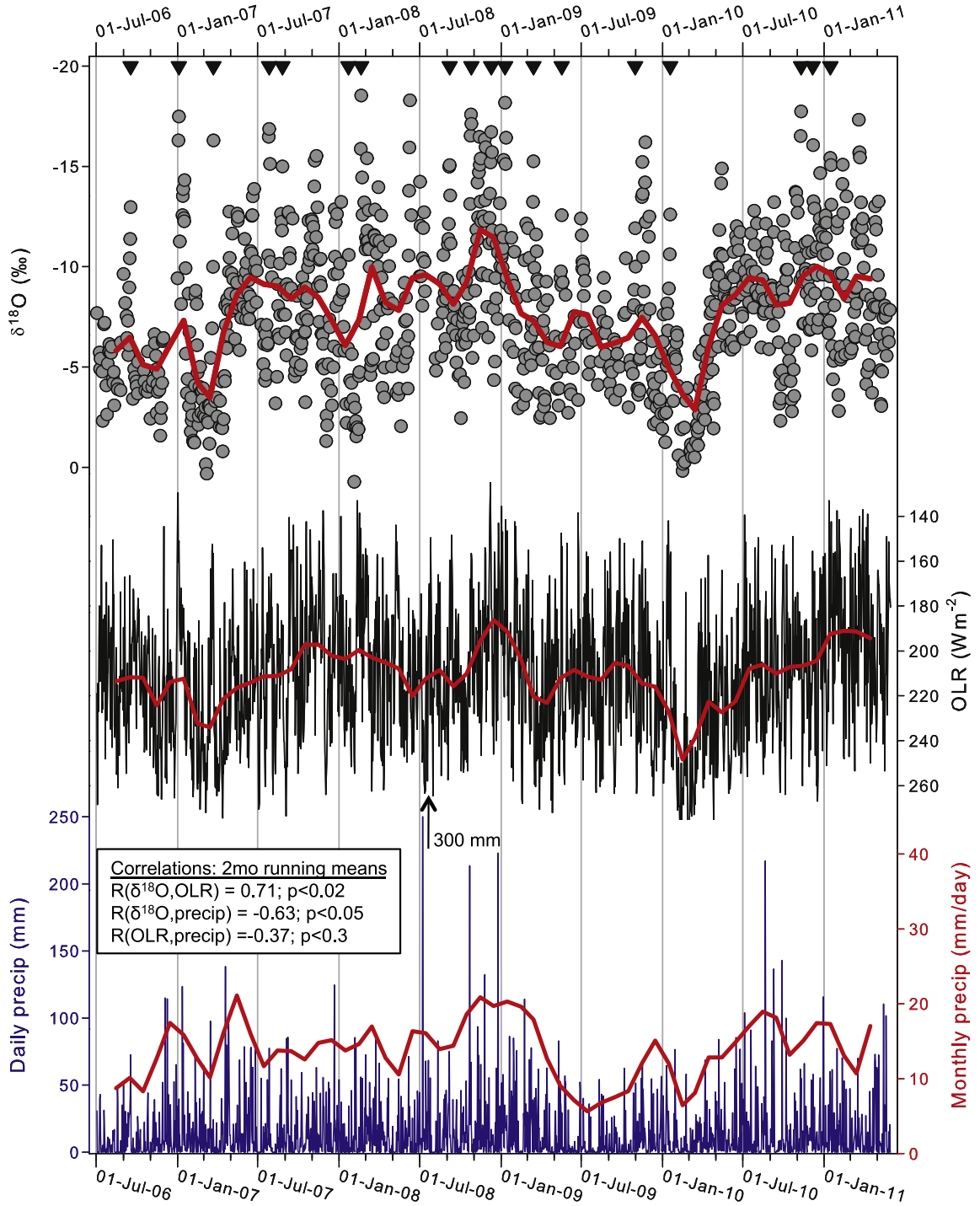

Fig. 3. (top) Timeseries of daily Mulu rainfall $\delta^{18}O$ (gray circles), plotted with a 2-month running mean (red line). Note that the 2-month running mean value plotted for December 2006 represents a linear interpolation of monthly values for November 2006 and January 2007. Intraseasonal rainfall $\delta^{18}O$ depletion events identified with our statistical filter (see Section 3.2.2) are denoted by black triangles along the upper *x*-axis. (middle) Daily NOAA interpolated OLR at 5°N, 115°E (black line), plotted with a 2-month running mean (red line). Axes for $\delta^{18}O$ and OLR are inverted. (bottom) Daily local Mulu precipitation amount (blue line), plotted with a 2-month running mean (red line, plotted on the right-hand *y*-axis). Note that one of the daily precipitation entries (300 mm) exceeds the scale plotted here, and is flagged accordingly. Correlations among the 2-month running means of the three timeseries are also provided. (For interpretation of the references to color in this figure legend, the reader is referred to the web version of this article.)

amount, and OLR across the duration of these events (Fig. 6). Rainfall $\delta^{18}O$ becomes gradually more depleted in the three days leading up to the minimum $\delta^{18}O$ value of $-15.4 \pm 2.4‰$ (1σ) on 'Day 0' in Fig. 6, and gradually returns to average values three days after peak $\delta^{18}O$ depletion. Local Mulu precipitation amount, however, is characterized by a more abrupt transition to above average precipitation rates, with a near doubling of the long-term average precipitation amount four days prior to the minimum rainfall $\delta^{18}O$ value. Precipitation rates remain anomalously high until 'Day 0', after which they abruptly drop to below average rates for 6 days. The temporal evolution of OLR across a rainfall $\delta^{18}O$ depletion event falls somewhere between that of rainfall $\delta^{18}O$ and local Mulu precipitation.

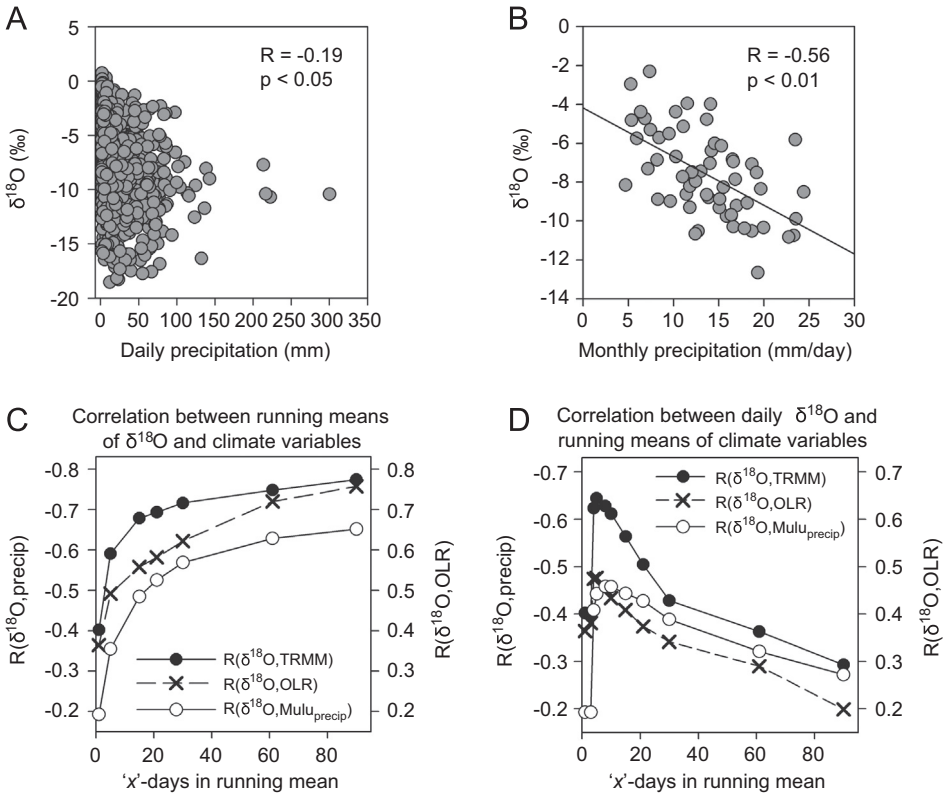

Fig. 4. (A) Relationship between daily Mulu rainfall $\delta^{18}O$ and daily Mulu precipitation amount. (B) Relationship between monthly-averaged Mulu rainfall $\delta^{18}O$ and monthly-averaged local Mulu precipitation amount. Solid black line represents linear best fit. (C) Correlation between '*x*'-day running mean Mulu rainfall $\delta^{18}O$ and '*x*'-day running means of Mulu precipitation amount (open circles, solid line), satellite-derived TRMM 3B42 precipitation amount (black circles, solid line), and NOAA interpolated OLR (black crosses, dashed line). (D) Correlation between daily Mulu rainfall $\delta^{18}O$ and '*x*'-day minus-projected running means of local Mulu precipitation amount (open circles, solid line), TRMM 3B42 precipitation amount (black circles, solid line), and OLR (black crosses, dashed line), after Risi et al. (2008a). TRMM and OLR in both (C) and (D) are spatial averages integrated over a $2.5^\circ \times 2.5^\circ$ gridbox centered about 5°N, 115°E.

The systematic relationships between Mulu rainfall $\delta^{18}O$, local Mulu precipitation, and OLR across the large rainfall $\delta^{18}O$ depletion events imply that they share a common origin. Indeed, a Hovmöller diagram of OLR confirms that the rainfall $\delta^{18}O$ depletion events occur during or immediately after the passage of organized regional convective activity from west to east (Fig. 7). The spatio-temporal signature of these OLR anomalies strongly resembles that of the MJO. Indeed, the majority of rainfall $\delta^{18}O$ depletion events do coincide with defined active (i.e. wet) phases of the MJO (Table S1). We conclude that the MJO strongly influences the intraseasonal variability of Mulu rainfall $\delta^{18}O$ and contributes to a "regional" amount effect relationship at intraseasonal timescales, as inferred by Cobb et al. (2007). In this case, the "regional" amount effect derives from the advection of depleted water vapor from regions to the west (upstream) of Mulu.

3.2.3. *Seasonal variability of rainfall $\delta^{18}O$*

Long-term monthly mean rainfall $\delta^{18}O$ values reveal a weak semi-annual seasonal cycle with an amplitude of ~2–3‰ that accounts for roughly 20% of the total variance in monthly rainfall $\delta^{18}O$ (Fig. 8). Two relative rainfall $\delta^{18}O$ minima occur in June–July and November–January, and two relative maxima occur in February–April and August–October. It is important to note that removing potential ENSO influences from the 5-yr rainfall $\delta^{18}O$ timeseries does not alter the rainfall $\delta^{18}O$ seasonal cycle (Fig. 8). Mulu rainfall $\delta^{18}O$ bears little resemblance to either local or regional precipitation on seasonal timescales, suggesting that seasonal variations in Mulu rainfall $\delta^{18}O$ are driven by a combination of more remote effects.

The semi-annual seasonal rainfall $\delta^{18}O$ composite presented here represents a significant revision to the annual seasonal cycle of rainfall $\delta^{18}O$ inferred by Cobb et al. (2007) from a much smaller sample size. Cobb et al. (2007) invoked seasonal changes in the degree of orographic fractionation to explain a relative $\delta^{18}O$ maximum (minimum) in boreal summer (winter). Such a mechanism may contribute to the complexity of seasonal rainfall $\delta^{18}O$ at Mulu, but our new results require a mechanism that leads to relatively high rainfall $\delta^{18}O$ values during the shoulder seasons of February/March/April and August/September/October (Fig. 8). Regional winds are relatively weak during these times, as the ITCZ transits directly over northern Borneo. We hypothesize that during these seasons, the adjoining sea surface is the dominant source of water vapor to Mulu, providing for shorter water vapor trajectories and therefore less cumulative isotopic fractionation. A detailed investigation of the causes of seasonal variations in Mulu rainfall $\delta^{18}O$, however, is beyond the scope of the present manuscript.

3.2.4. *Interannual variability of rainfall $\delta^{18}O$*

The 5-yr Mulu rainfall $\delta^{18}O$ timeseries contains appreciable interannual variations of 6–8‰ that account for approximately 70% of the total monthly variance in rainfall $\delta^{18}O$. Interannual rainfall $\delta^{18}O$ variations are significantly correlated to both local Mulu precipitation ($R=-0.63$, $p<0.05$; Fig. 9A) and large-scale ENSO indices (e.g. $R=0.64$, $p<0.05$ for NIÑO4; Fig. 9C). Compared to western Pacific ENSO indices, eastern Pacific indices are more weakly correlated to Mulu rainfall $\delta^{18}O$ (Table S3). Local Mulu precipitation amount is characterized by lower correlations to ENSO indices (e.g. $R=-0.50$, $p<0.1$ for NIÑO4; Fig. 9F). These findings strongly suggest that, compared

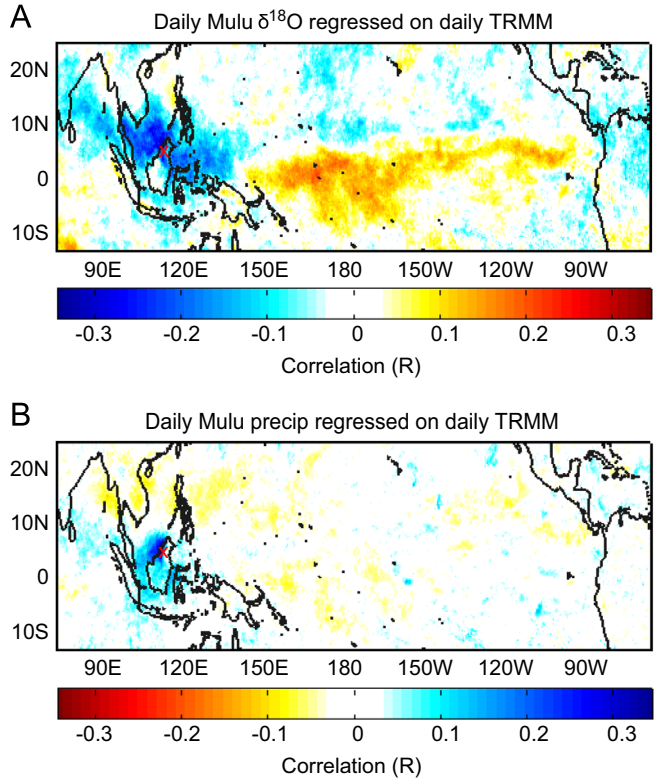

Fig. 5. Correlation maps of daily Mulu rainfall $\delta^{18}O$ and local Mulu precipitation amount with daily TRMM precipitation product 3B42 for July 2006–May 2011 constructed using ordinary least squares regression. (A) Correlation between daily Mulu rainfall $\delta^{18}O$ and gridded TRMM precipitation. (B) Same as (A) but with daily local Mulu precipitation amount. The red 'x' in each panel marks the location of our study site at Gunung Mulu National Park (4°N, 114°E).

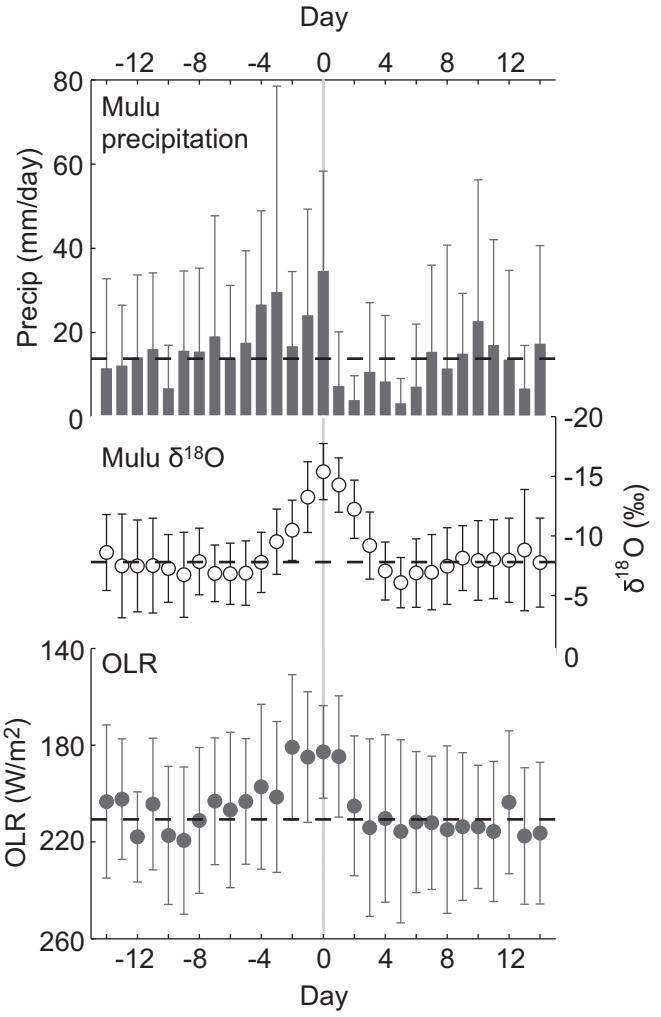

Fig. 6. Composites of (top) daily Mulu precipitation amount, (middle) daily Mulu rainfall $\delta^{18}O$, and (bottom) daily OLR at 5°N, 115°E during the eighteen intraseasonal rainfall $\delta^{18}O$ depletion events centered about Day '0', which represents the minimum rainfall $\delta^{18}O$ value of the depletion events. Error bars reflect the 1σ spread for each daily average. Dashed horizontal lines represent the long-term daily average value of each parameter over the 5-yr study period (13.8 ± 23.2 mm/day [1σ] for local Mulu precipitation, -7.8 ± 3.6‰ [1σ] for Mulu rainfall $\delta^{18}O$, and 210.7 ± 30.4 Wm^{-2} [1σ] for OLR). Note that axes for $\delta^{18}O$ and OLR are inverted.

to Mulu precipitation, Mulu rainfall $\delta^{18}O$ is a better tracer of ENSO variability, owing to its time- and space-integrative properties.

Regression maps of Mulu rainfall $\delta^{18}O$ and basin-scale precipitation (Fig. 10A) and OLR (Fig. 10B) reveal significant correlations that extend from the western to central Pacific. The spatial pattern of these correlations strongly resembles the first EOF of global precipitation, which is attributed to ENSO variability (e.g. Fig. 1 of Furtado et al., 2009). These results support the existence of a strong "regional" amount effect associated with ENSO variability, whereby regionally suppressed convection in the western Pacific leads to higher rainfall isotopes during El Niño conditions, and vice versa during La Niña events. It is worth noting that these statistically robust relationships were extracted from a time series that contained only one "strong" ENSO event (i.e. the 2010/2011 La Niña), thus underscoring the sensitivity of rainfall $\delta^{18}O$ at our site to small/moderate changes in the ENSO state.

In contrast to Mulu rainfall $\delta^{18}O$, which closely tracks basin-scale ocean–atmosphere interactions associated with ENSO, Mulu precipitation amount is correlated to regional precipitation in a much smaller area (Figs. 10C, D). The fact that Mulu rainfall $\delta^{18}O$ is more sensitive than Mulu precipitation amount to basin-scale ENSO variability indicates that the rainfall $\delta^{18}O$–ENSO relationship is primarily transmitted through regional-scale, rather than local, convective activity. In other words, interannual variations in the overall convective state of the WPWP imprint water vapor with an isotopic ENSO signal prior to the vapor's arrival at northern Borneo, while ENSO-related changes in convective activity at our site may subsequently serve to amplify the far-field ENSO signal in rainfall $\delta^{18}O$.

4. Discussion

4.1. Spatial and temporal signatures of the amount effect

Across nearly all timescales studied, Mulu rainfall $\delta^{18}O$ is inversely related to precipitation variability, consistent with the tropical amount effect. While we find evidence for a "local" amount effect across a single convective event, we demonstrate that rainfall $\delta^{18}O$ variability on diurnal to interannual timescales at Mulu is tied to a "regional" amount effect.

Within an individual storm, we find evidence that local processes, specifically below-cloud evaporation of falling raindrops, cause the observed inverse correlation between rainfall $\delta^{18}O$ and precipitation rate. This relationship arises because the degree of kinetic fractionation during the evaporation of a raindrop depends on the humidity of the atmosphere through which it falls, with higher humidity suppressing evaporative enrichment (Dansgaard, 1964; Stewart, 1975). The response of rainfall $\delta^{18}O$ to changes in the efficiency of below-cloud evaporation is essentially instantaneous at the intra-storm timescale. These findings provide

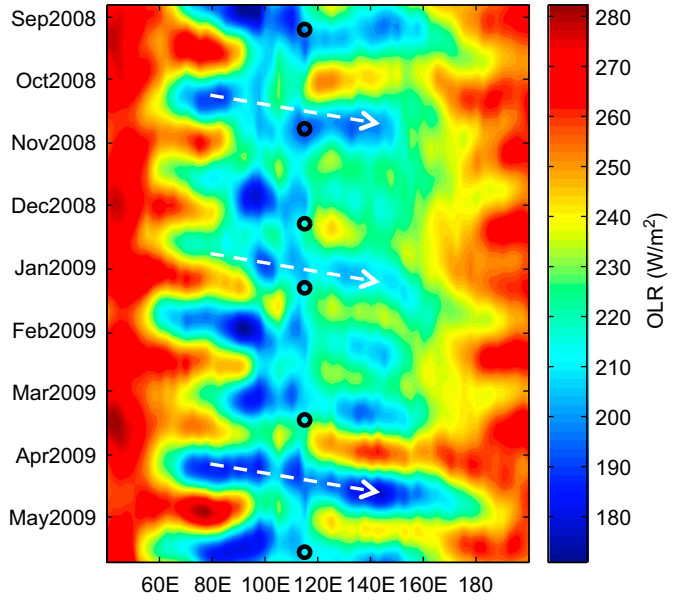

Fig. 7. Time-longitude map of daily NOAA interpolated OLR filtered with a 30–96 day bandpass filter and averaged over 0–5°N for the time window spanning 8/26/2008–5/23/2009. Open circles mark the timing of intraseasonal rainfall $\delta^{18}O$ depletion events that occur during the time window. White dashed arrows highlight examples of eastward-propagating enhanced convection.

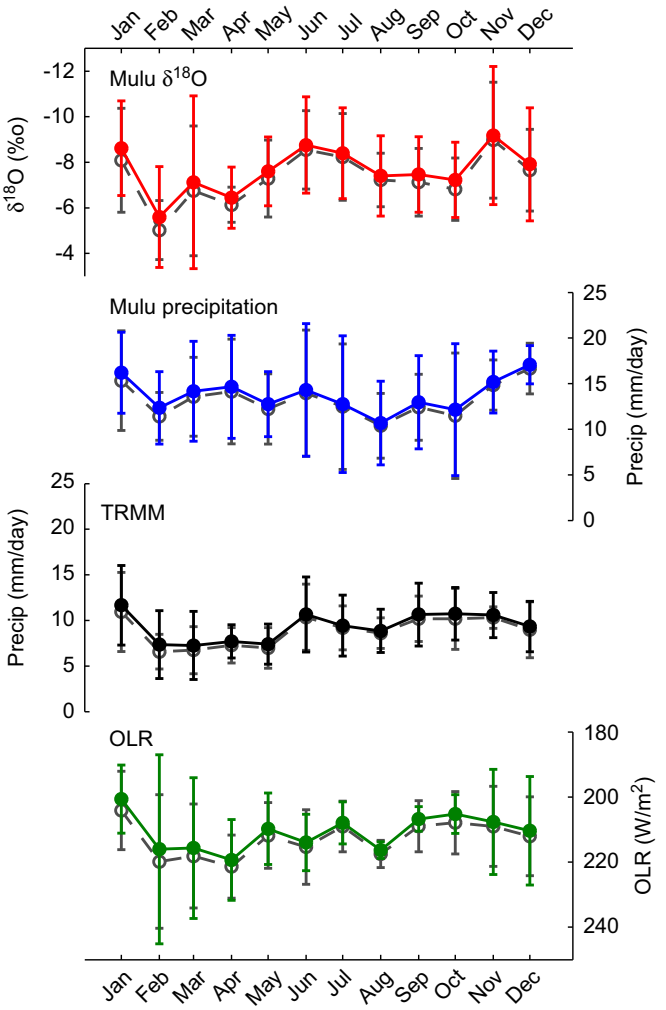

Fig. 8. Long-term monthly mean Mulu rainfall $\delta^{18}O$ (red), local Mulu precipitation amount (blue), satellite-measured TRMM 3B43 precipitation amount (black), and NOAA interpolated OLR (green) from July 2006 to May 2011. TRMM and OLR are spatial averages integrated over a $2.5^\circ \times 2.5^\circ$ gridbox centered about 5°N, 115°E. Also plotted are versions of each long-term monthly mean with ENSO-related variability removed (gray). Error bars represent the 1σ spread of each month's mean value. Note that axes for $\delta^{18}O$ and OLR are inverted. (For interpretation of the references to color in this figure legend, the reader is referred to the web version of this article.)

observational confirmation of numerical modeling results invoking post-condensation evaporative enrichment as a primary control on rainfall isotopes during individual precipitation events (Lee and Fung, 2008; Risi et al., 2008a).

At the diurnal timescale, several lines of evidence suggest that isotopic fractionation associated with the "local" amount effect is dwarfed by $\delta^{18}O$ variations that reflect regional convective activity. For one, our results indicate that post-condensation evaporation of falling raindrops, which amounts to fractionations of ~1–2‰ within the March 7, 2010 convective event, is relatively small compared to day-to-day rainfall $\delta^{18}O$ variations of ~2–10‰. Indeed, previous observational and GCM-based studies also find that local post-condensation evaporation has relatively little impact on rainfall $\delta^{18}O$ values on daily and longer timescales in wet tropical regions (Kurita et al., 2009; Breitenbach et al., 2010; Field et al., 2010). Secondly, the weak correlation between daily rainfall $\delta^{18}O$ and daily Mulu precipitation amount further suggests that local rainout has relatively little impact on cumulative daily Mulu rainfall $\delta^{18}O$ values. Similarly weak correlations between daily rainfall $\delta^{18}O$ and local precipitation amount are also observed at other tropical and subtropical sites (e.g. Yamanaka et al., 2004; Risi et al., 2008b, Kurita et al., 2009, Breitenbach et al., 2010; Vimeux et al., 2011).

The weak daily rainfall $\delta^{18}O$–precipitation relationship can be attributed to the time- and space-integrative properties of rainfall $\delta^{18}O$, illustrated by the high correlation between daily rainfall $\delta^{18}O$ and regional precipitation amount averaged over the preceding week (Fig. 4D). The 5–8-day vapor residence time that we observe at Mulu suggests that isotopic signals persist within the atmospheric vapor above Mulu for several days. These findings are consistent with those of studies at other tropical sites, which explain the time-integrative behavior of rainfall $\delta^{18}O$ via a repeated atmospheric vapor recycling process, in which low-level vapor depleted by earlier convective activity is fed into successive convective systems (Risi et al., 2008a, 2008b; Vimeux et al., 2011). In this way, the isotopic composition of the recycled water vapor – and that of the resultant rainfall – reflects the cumulative intensity of the previous days' convective activity, thus causing daily rainfall $\delta^{18}O$ to be poorly correlated with daily precipitation amount. Taken together, these results suggest that diurnal rainfall $\delta^{18}O$ variability at our site is more dependent on the isotopic composition of the water vapor from which it condenses than the local fractionation processes that occur during individual rainfall events. The space-integrative property of daily Mulu rainfall $\delta^{18}O$, illustrated by the strong correlations between Mulu rainfall $\delta^{18}O$ and regional precipitation amount in Fig. 4C and D, suggests that Mulu vapor $\delta^{18}O$ is also significantly influenced by regional-scale convective processes. This is further supported by Fig. 5, which shows that correlations between daily gridded TRMM precipitation amount and daily Mulu rainfall $\delta^{18}O$ are far more regionally extensive than they are for daily Mulu precipitation amount.

The large multi-day rainfall $\delta^{18}O$ depletion events observed at Mulu typically coincide with the passage of mesoscale convective systems associated with the MJO (Fig. 7). We infer that these large-scale convective systems deliver anomalously depleted water vapor $\delta^{18}O$ to Mulu, thus resulting in depleted rainfall $\delta^{18}O$. Indeed, Kurita et al. (2011) and Berkelhammer et al. (2012) observe

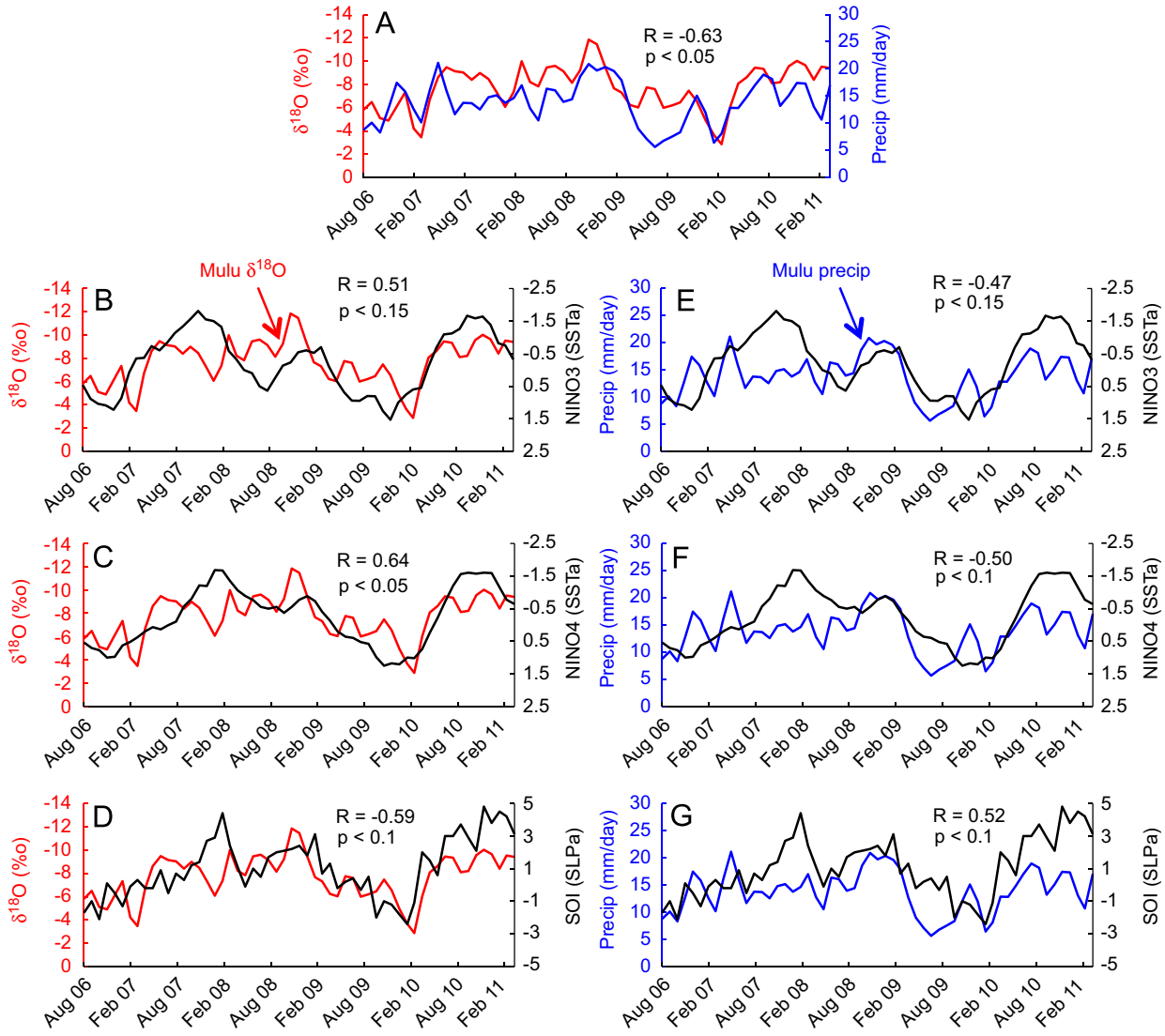

Fig. 9. (A) Timeseries of 2-month running mean Mulu rainfall $\delta^{18}O$ and local Mulu precipitation amount. (B–D) Comparisons of 2-month running mean Mulu rainfall $\delta^{18}O$ with (B) NIÑO3, (C) NIÑO4, and (D) SOI. (E–G) Same as (B–D) but for 2-month running mean Mulu precipitation amount. Axes for rainfall $\delta^{18}O$ and NIÑO indices are inverted (with the exception of SOI). NIÑO and SOI indices obtained from http://www.cpc.ncep.noaa.gov/data/indices/.

large negative anomalies in water vapor δD as active MJO events pass over the northern Borneo area. However, the most depleted Mulu rainfall $\delta^{18}O$ occurs towards the end of the passage of a regional convective system rather than at the onset (Figs. 6 and 7). Risi et al. (2008b) similarly observe a multi-day delay in maximum rainfall $\delta^{18}O$ depletion with respect to the onset of enhanced convective activity associated with the monsoon in west Africa. In our case, maximum rainfall $\delta^{18}O$ depletion occurs after ~3–4 days of above-average local precipitation. As water vapor residence times are 5–8 days at our site, this relatively rapid depletion suggests that additional vapor fractionation occurs as a result of on-site convective activity. Thus, the largest, sharpest rainfall $\delta^{18}O$ depletions observed in our timeseries can be ascribed to two processes: (1) regionally-enhanced convection associated with the MJO delivers already depleted water vapor to Gunung Mulu, and (2) intense local convective activity distills the vapor pool over a period of several days, amplifying the advected negative isotopic anomaly. In this way, Mulu rainfall $\delta^{18}O$ variations on intraseasonal timescales reflect contributions from both regional and local convective activity.

The close relationship between regional hydrology and Mulu rainfall $\delta^{18}O$ is most evident on interannual timescales, when weak to moderate El Niño events are associated with significantly higher rainfall $\delta^{18}O$ at Mulu, and vice versa during La Niña events. In this context, it is striking that Mulu rainfall $\delta^{18}O$ is a better indicator than local Mulu precipitation of basin-scale atmospheric circulation on interannual timescales. This reinforces the notion that water vapor $\delta^{18}O$ has an integrating effect, averaging the convective activity experienced during its transport history through both space and time. As such, the ENSO signal captured by Mulu rainfall $\delta^{18}O$ reflects the sensitivity of Mulu rainfall $\delta^{18}O$ to regional climatic conditions on monthly timescales.

4.2. *Implications for $\delta^{18}O$–based paleoclimate reconstructions*

The present study demonstrates that changes in regional convective activity are reflected in rainfall $\delta^{18}O$ variations at our site, providing further empirical support for the amount effect framework used to interpret $\delta^{18}O$-based paleo-reconstructions from northern Borneo stalagmites (Partin et al., 2007; Meckler et al., 2012). As such, any changes over time in the background state of regional-scale hydrology, such as variability in the strength and/or location of deep convection in the WPWP, would likely impact rainfall $\delta^{18}O$ at Mulu. More generally, the ability of rainfall

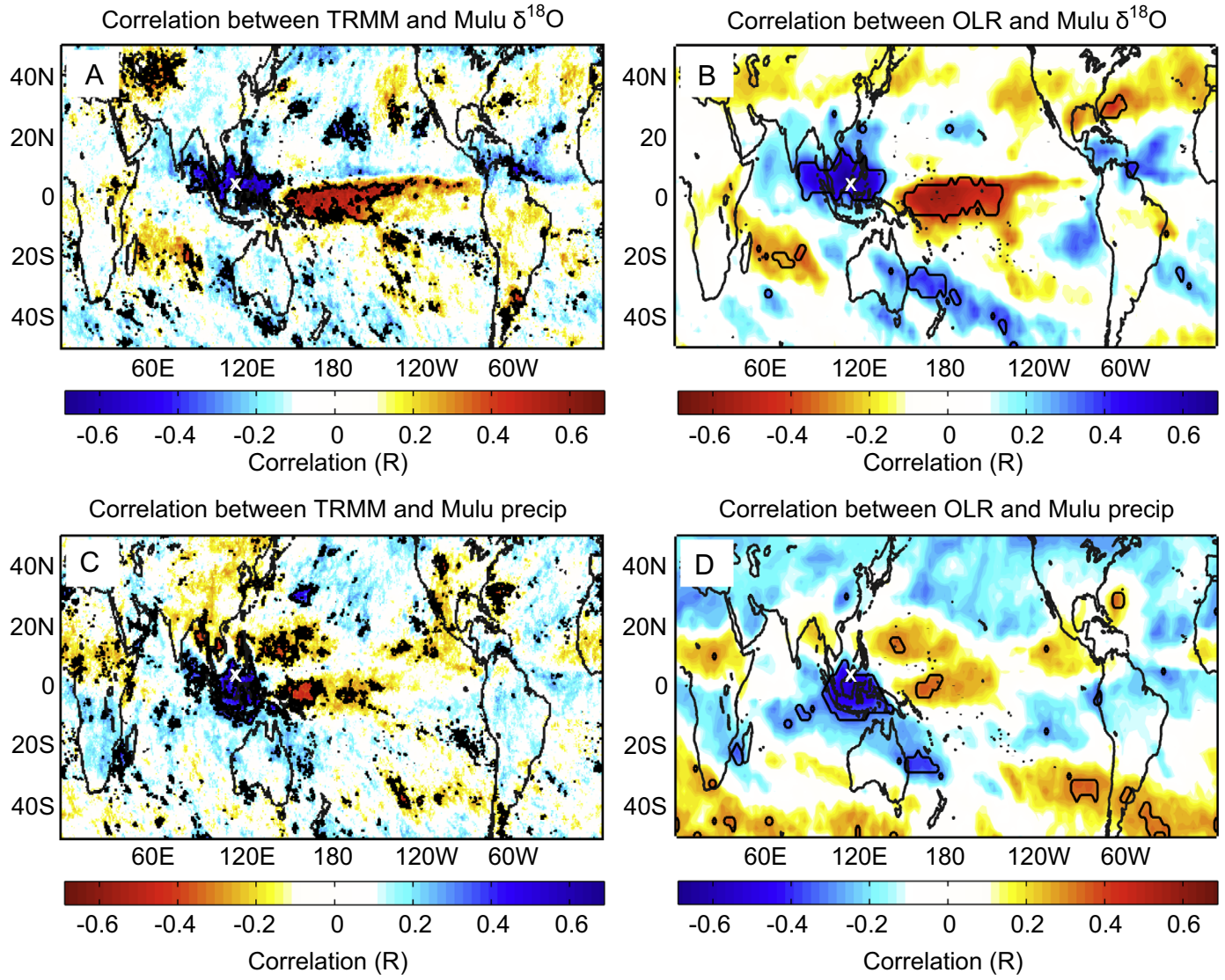

Fig. 10. Correlation maps of monthly mean Mulu rainfall $\delta^{18}O$ and local Mulu precipitation amount with monthly TRMM precipitation product 3B43 and monthly NOAA interpolated OLR for July 2006–May 2011 constructed using ordinary least squares regression. (A) Correlation between monthly mean Mulu rainfall $\delta^{18}O$ and gridded TRMM precipitation. (B) Same as (A) but with gridded OLR. (C) Correlation between monthly mean Mulu precipitation amount and gridded TRMM precipitation. D) Same as (C) but with gridded OLR. Black contour lines indicate 95% significance regions as determined by the student's *t*-test using effective degrees of freedom (Bretherton et al., 1999). The white 'x' in each panel marks the location of our study site at Gunung Mulu National Park (4°N, 114°E). Color scales for panels (B) and (C) are inverted. (For interpretation of the references to color in this figure legend, the reader is referred to the web version of this article.)

$\delta^{18}O$ to integrate regional convective activity across space and time makes it a much better indicator of large-scale hydrology than local precipitation amount, which contains much more noise. Therefore, while precipitation variability from nearby sites may be poorly correlated (Dayem et al., 2010), rainfall $\delta^{18}O$ variability from nearby sites may indeed be highly correlated due to the integrative properties of rainfall $\delta^{18}O$. This explains why stalagmite $\delta^{18}O$ records from caves that are hundreds of kilometers apart reflect the same regional-scale hydroclimate influences (e.g. Yuan et al., 2004; Wang et al., 2001). Likewise, well-reproduced cave stalagmite records from a single site can be interpreted as robust indicators of regional-scale hydroclimate variability (e.g. Partin et al., 2007).

When considering how to relate rainfall $\delta^{18}O$ variability to stalagmite calcite $\delta^{18}O$ variability, one must keep in mind that several processes mediate the cloud-to-calcite transformation of rainfall $\delta^{18}O$ signals. First, the infiltration of rainwaters through the karst environment inevitably leads to some measure of signal attenuation from mixing, as well as signal delay depending on water residence times in the karst. In comparing several Mulu dripwater $\delta^{18}O$ timeseries with rainfall $\delta^{18}O$ timeseries, Cobb et al. (2007) argue for dripwater residence times of 2–3 months, based on the preservation of a weak seasonal cycle in dripwater $\delta^{18}O$. However, owing to logistical difficulties in collecting timeseries of dripwater $\delta^{18}O$ from slow to ultra-slow drips that typically form stalagmites, residence time estimates for the most relevant drips remain poorly constrained. A new 5-yr-long timeseries of dripwater $\delta^{18}O$ from both fast and slow Mulu drips will help quantify groundwater transit times across a broad range of drip environments (Moerman et al., 2012). A complementary approach involves pursuing a "calibration" of annual to sub-annual stalagmite $\delta^{18}O$ with climatic timeseries over the 20th century. The latter approach requires unusually fast-growing stalagmites and small chronological errors afforded by either annual layer counting and/or many U/Th dates (e.g. Frappier et al., 2002, 2007; Fleitmann et al., 2004; Treble et al., 2005) and, as such, are relatively rare.

Such calibrations generally confirm the interpretation of stalagmite $\delta^{18}O$ reconstructions as hydroclimate reconstructions, but highlight key uncertainties surrounding the cloud-to-calcite transformation of rainfall $\delta^{18}O$ signals.

Our study suggests that as records of paleo-rainfall $\delta^{18}O$, stalagmite $\delta^{18}O$ records reflect changes in regional convective activity, which in turn is related to a variety of climatic processes operating across a range of timescales. The Mulu rainfall $\delta^{18}O$ timeseries exhibits variability at intraseasonal, seasonal, and interannual timescales, each linked to a distinct climatic phenomenon. Therefore, low-frequency stalagmite $\delta^{18}O$ signals at Mulu could conceivably represent a change in the frequency and/or amplitude of MJO-related variability, a change in the seasonal rainfall cycle (i.e. the ITCZ), and/or a change in the tropical Pacific's zonal SST gradient (i.e. ENSO). This ambiguity illustrates the need to transition from reliance on single-site stalagmite $\delta^{18}O$ reconstructions to networks of paleoclimate records that span the geographic range of the climatic phenomenon of interest. Indeed, small networks of stalagmite $\delta^{18}O$ records have recently been applied to investigate changes in the ITCZ by Griffiths et al. (2009) with a north-south transect from southeast Asia to Indonesia. Such an approach could be used to investigate changes in the zonal convective gradient across the equatorial tropical Pacific. Networks such as these would provide important benchmarks for newly available paleoclimate simulations of coupled GCMs, some of which are equipped with water isotope modules (e.g. LeGrande et al., 2006; Sturm et al., 2010; Risi et al., 2010). Such data-model comparisons provide an opportunity to advance our understanding of the mechanisms of global climate change on decadal to millennial timescales and how well these processes are represented in state-of-the-art climate models.

5. Conclusions

Our analyses demonstrate that the inverse relationship between rainfall $\delta^{18}O$ and precipitation amount, known as the amount effect, is a strong control on the oxygen isotopic composition of rainfall in northern Borneo over the majority of the timescales examined. Studying a single precipitation event at high temporal resolution, we find evidence for local fractionation processes driving intra-storm rainfall $\delta^{18}O$ variability, whereas the majority of diurnal to interannual rainfall $\delta^{18}O$ variability originates from regional-scale hydrological processes. Daily rainfall $\delta^{18}O$ variations best reflect cumulative regional precipitation occurring over the preceding week. Intraseasonal rainfall $\delta^{18}O$ variability, which is particularly large at our site with up to $\sim$16‰ shifts, is closely associated with the MJO – the dominant mode of intraseasonal climatic variability in the tropics – and exhibits influences from both local and far-field fractionation processes. Interannual rainfall $\delta^{18}O$ variability at Mulu is significantly correlated to ENSO, whereby a basin-scale reorganization of atmospheric circulation patterns during El Niño and La Niña events affects regional convective activity and in turn the regional isotopic composition of the atmospheric water vapor. In this context, Mulu rainfall $\delta^{18}O$ is superior to local Mulu precipitation amount as a proxy for ENSO variability.

Our study documents a robust amount effect relationship between regional precipitation and Mulu rainfall $\delta^{18}O$ that is most evident at intraseasonal and interannual timescales. Our results lend strong support to the interpretation of $\delta^{18}O$-based reconstructions from northern Borneo stalagmites as regional hydroclimate proxies, with significant influences from intraseasonal and interannual variability, and to a lesser extent, seasonal variability. More generally, our study illustrates that the processes governing the climate–rainfall $\delta^{18}O$ relationship are space- and time-dependent. As such, our results support the generation of multi-year, daily-resolved timeseries of rainfall isotopes in order to identify the dynamical controls on rainfall $\delta^{18}O$ variability at sites where accurate interpretations of paleoclimate $\delta^{18}O$ reconstructions are especially critical.

Acknowledgments

The authors gratefully acknowledge the Mulu Meteorological Station staff for overseeing the collection of the daily rainfall samples, as well as Jenny Malang, Syria Lejau, and the staff at Gunung Mulu National Park for their dedicated assistance during fieldtrips. Permits for this work were granted by the Malaysian Economic Planning Unit, the Sarawak State Planning Unit, and the Sarawak Forestry Department. We also thank Aaron van Pelt of Picarro, Inc., Bruce Vaughn of INSTARR at UC Boulder, and Krystle Stewart for their invaluable assistance during sample analysis and Dr. Emanuele Di Lorenzo for his assistance with the TRMM dataset. This research was supported by NSF Grant 0645291 to KMC, and JWM was funded by a NSF Graduate Research Fellowship.

Appendix A. Supporting information

Supplemental Section and full Mulu rainfall $\delta^{18}O$ dataset can be found in the online version at http://dx.doi.org/10.1016/j.epsl.2013.03.014. The full Mulu rainfall $\delta^{18}O$ dataset may also be retrieved from the Global Network of Isotopes in Precipitation (GNIP), available via IAEA's WISER database at http://www.iaea.org/water.

References

Aggarwal, P., Frohlich, K., Kulkarni, K., Gourcy, L., 2004. Stable isotope evidence for moisture sources in the Asian summer monsoon under present and past climate regimes. Geophys. Res. Lett. 31, L08203.

Araguas-Araguas, L., Froehlich, K., Rozanski, K., 1998. Stable isotope composition of precipitation over southeast Asia. J. Geophys. Res. Atmos. 103, 28721–28742.

Arkin, P.A., Ardanuy, P.E., 1989. Estimating climatic-scale precipitation from space: a review. J. Clim. 2, 1229–1238.

Bar-Matthews, M., Ayalon, A., Kaufman, A., 1997. Late Quaternary paleoclimate in the Eastern Mediterranean region from stable isotope analysis of speleothems at Soreq Cave. Isr. Quat. Res 47, 155–168.

Bell, G.D., Halpert, M.S., 1998. Climate assessment for 1997. Bull. Am. Meteorol. Soc. 79 1014–1014.

Berkelhammer, M., Risi, C., Kurita, N., Noone, D., 2012. The moisture source and sequence for the Madden–Julian Oscillation as derived from satellite retrievals of HDO and H_2O. J. Geophys. Res 117, D03106.

Breitenbach, S., Adkins, J., Meyer, H., Marwan, N., Kumar, K., Haug, G., 2010. Strong influence of water vapor source dynamics on stable isotopes in precipitation observed in Southern Meghalaya, NE India. Earth Planet. Sci. Lett. 292, 212–220.

Bretherton, C.S., Widmann, M., Dymnikov, V.P., Wallace, J.M., Bladè, I., 1999. Effective number of degrees of freedom of a spatial field. J. Clim. 12, 1990–2009.

Burns, S.J., Matter, A., Frank, N., Mangini, A., 1998. Speleothem-based paleoclimate record from northern Oman. Geology 26 (6), 499–502.

Carolin, S.A., Cobb, K.M., Adkins, J.F., Clark, B., Conroy, J.L., Lejau, S., Malang, J., Tuen, A.A., Varied response of western Pacific hydrology to climate forcings over the last glacial period. Science, in press.

Celle-Jeanton, H., Gonfiantini, R., Travi, Y., Sol, B., 2004. Oxygen-18 variations of rainwater during precipitation: application of the Rayleigh model to selected rainfalls in southern France. J. Hydrol. 289, 165–177.

Cobb, K.M., Adkins, J.F., Partin, J.W., Clark, B., 2007. Regional-scale climate influences on temporal variations of rainwater and cave dripwater oxygen isotopes in northern Borneo. Earth Planet. Sci. Lett. 263, 207–220.

Conroy, J.L., Cobb, K.M., Noone, D., Comparison of precipitation isotope variability across the tropical Pacific in observations and SWING2 model simulations. J. Geophys. Res. Atmos., http://dx.doi.org/10.1002/jgrd.50412, in press.

Craig, H., 1961. Isotopic variations in meteoric waters. Science 133, 1702–1703.

Dansgaard, W., 1964. Stable isotopes in precipitation. Tellus 16 (4), 436–468.

Dayem, K., Molnar, P., Battisti, D., Roe, G., 2010. Lessons learned from oxygen isotopes in modern precipitation applied to interpretation of speleothem records of paleoclimate from eastern Asia. Earth Planet. Sci. Lett. 295, 219–230.

Dykoski, C.A., Edwards, R.L., Cheng, H., Yuan, D.X., Cai, Y.J., Zhang, M.L., Lin, Y.S., Qing, J.M., An, Z.S., Revenaugh, J., 2005. A high-resolution, absolute-dated Holocene and deglacial Asian monsoon record from Dongge Cave, China. Earth Planet. Sci. Lett. 233, 71–86.
Field, R., Jones, D., Brown, D., 2010. Effects of postcondensation exchange on the isotopic composition of water in the atmosphere. J. Geophys. Res. 115, D24305.
Fleitmann, D., Burns, S.J., Neff, U., Mudelsee, M., Mangini, A., Matter, A., 2004. Palaeoclimatic interpretation of high-resolution oxygen isotope profiles derived from annually laminated speleothems from Southern Oman. Quat. Sci. Rev. 23, 935–945.
Frappier, A., Sahagian, D., Gonzalez, L.A., Carpenter, S.J., 2002. El Niño events recorded by stalagmite carbon isotopes. Science 298, 565.
Frappier, A., Sahagian, D., Carpenter, S., Gonzalez, L., Frappier, B., 2007. Stalagmite stable isotope record of recent tropical cyclone events. Geology 35 (2), 111–114.
Furtado, J.C., Di Lorenzo, E., Cobb, K.M., Bracco, A., 2009. Paleoclimate reconstructions of tropical sea surface temperatures from precipitation proxies: methods, uncertainties, and nonstationarity. J. Clim 22, 1104–1123.
Gao, J., Masson-Delmotte, V., Yao, T., Tian, L., Risi, C., Hoffmann, G., 2011. Precipitation water stable isotopes in the south Tibetan plateau: observations and modeling. J. Clim. 24, 3161–3178.
Gat, J.R., 1996. Oxygen and hydrogen isotopes in the hydrologic cycle. Annu. Rev. Earth Planet. Sci. 24, 225–262.
Griffiths, M., Drysdale, R., Gagan, M., Zhao, J.-x., Ayliffe, L., Hellstrom, J., Hantoro, W., Frisia, S., Feng, Y.-x., Cartwright, I., St. Pierre, E., Fischer, M., Suwargadi, B., 2009. Increasing Australian-Indonesian monsoon rainfall linked to early Holocene sea-level rise. Nat. Geosci. 2, 636–639.
Hoffmann, G., Werner, M., Heimann, M., 1998. Water isotope module of the ECHAM atmospheric general circulation model: a study on timescales from days to several years. J. Geophys. Res. Atmos. 103, 16871–16896.
Hoffmann, G., Ramirez, E., Taupin, J., Francou, B., Ribstein, P., Delmas, R., Dürr, H., Gallaire, R., Simões, J., Schotterer, U., Stievenard, M., Werner, M., 2003. Coherent isotope history of Andean ice cores over the last century. Geophys. Res. Lett. 30 (4), 1179.
Huffman, G., Adler, R., Bolvin, D., Gu, G., Nelkin, E., Bowman, K., Hong, Y., Stocker, E., Wolff, D., 2007. The TRMM multisatellite precipitation analysis (TMPA): Quasi-global, multiyear, combined-sensor precipitation estimates at fine scales. J. Hydrometeorol. 8, 38–55.
International Atomic Energy Agency, 2006. Isotope Hydrology Information System. The ISOHIS Database. Available from: ⟨http://isohis.iaea.org⟩.
Joussaume, S., Sadourny, R., Jouzel, J., 1984. A general-circulation model of water isotope cycles in the atmosphere. Nature 311, 24–29.
Jouzel, J., Russell, G.L., Suozzo, R.J., Koster, R.D., White, J.W.C., Broecker, W.S., 1987. Simulations of the HDO and H2 O-18 atmospheric cycles using the NASA GISS general-circulation model—the seasonal cycle for present-day conditions. J. Geophys. Res. Atmos. 92 (D12), 14739–14760.
Kurita, N., Ichiyanagi, K., Matsumoto, J., Yamanaka, M., Ohata, T., 2009. The relationship between the isotopic content of precipitation and precipitation amount in tropical regions. J. Geochem. Explor. 102, 113–122.
Kurita, N., Noone, D., Risi, C., Schmidt, G.A., Yamada, H., Yoneyama, K., 2011. Intraseasonal isotopic variation associated with the Madden–Julian Oscillation. J. Geophys. Res. 116, D24101.
Lawrence, J., Gedzelman, S., 1996. Low stable isotope ratios of tropical cyclone rains. Geophys. Res. Lett. 23 (5), 527–530.
Lawrence, J.R., Gedzelman, S.D., Dexheimer, D., Cho, H.K., Carrie, G.D., Gasparini, R., Anderson, C.R., Bowman, K.P., Biggerstaff, M.I., 2004. Stable isotopic composition of water vapor in the tropics. J. Geophys. Res. Atmos. 109, D06115.
Lee, J.-E., Fung, I., DePaolo, D., Henning, C., 2007. Analysis of the global distribution of water isotopes using the NCAR atmospheric general circulation model. J. Geophys. Res. 112, D16306.
Lee, J.-E., Fung, I., 2008. "Amount effect" of water isotopes and quantitative analysis of post-condensation processes. Hydrol. Processes 22, 1–8.
Lee, J.-E., Johnson, K., Fung, I., 2009. Precipitation over South America during the Last Glacial Maximum: an analysis of the "amount effect" with a water isotope-enabled general circulation model. Geophys. Res. Lett. 36, L19701.
LeGrande, A., Schmidt, G., Shindell, D., Field, C., Miller, R., Koch, D., Faluvegi, G., Hoffmann, G., 2006. Consistent simulations of multiple proxy responses to an abrupt climate change event. Proc. Natl. Acad. Sci. 103, 837–842.
LeGrande, A., Schmidt, G., 2009. Sources of Holocene variability of oxygen isotopes in paleoclimate archives. Clim. Past 5, 441–445.
Lewis, S., LeGrande, A., Kelley, M., Schmidt, G., 2010. Water vapor source impacts on oxygen isotope variability in tropical precipitation during Heinrich events. Clim. Past 6, 325–340.
Liebmann, B, Smith, C., 1996. Description of a complete (interpolated) outgoing longwave radiation dataset. Bull. Am. Meteorol. Soc. 77, 1275–1277.
Madden, R.A., Julian, P.R., 1972. Description of global-scale circulation cells in tropics with a 40–50day period. J. Atmos. Sci. 29, 1109–1123.
Meckler, A., Clarkson, M., Cobb, K., Sodemann, H., Adkins, J., 2012. Interglacial hydroclimate in the tropical west Pacific through the late Pleistocene. Science 336, 1301–1304.
Moerman, J.W., Cobb, K.M., Adkins, J.F., Sodemann, H., Clark, B., Tuen, A.A., 2012. Local and regional climatic controls on high-resolution rainfall and cave dripwater oxygen isotopes in northern Borneo. Abstract PP33A-2094 presented at 2012 Fall Meeting American Geophysical Union, San Francisco, CA, 3–7 Dec.
Noone, D., Simmonds, I., 2002. Associations between delta O-18 of water and climate parameters in a simulation of atmospheric circulation for 1979–95. J. Clim. 15, 3150–3169.
Partin, J.W., Cobb, K.M., Adkins, J.F., Fernandez, D.P., Clark, B., 2007. Millennial-scale trends in West Pacific Warm Pool hydrology from the Last Glacial Maximum to present. Nature 499, 452–455.
Rasmusson, E.M., Wallace, J.M., 1983. Meteorological aspects of the El Niño/Southern Oscillation. Science 222, 1195–1202.
Reynolds, R.W., Rayner, N.A., Smith, T.M., Stokes, D.C., Wang, W., 2002. An improved in situ and satellite SST analysis for climate. J. Clim. 15, 1609–1625.
Risi, C., Bony, S., Vimeux, F., 2008a. Influence of convective processes on the isotopic composition (δ18O and δD) of precipitation and water vapor in the Tropics, Part 2: physical interpretation of the amount effect. J. Geophys. Res. 113, D19306.
Risi, C., Bony, S., Vimeux, F., Descroix, L., Boubacar, I., Lebreton, E., Mamadou, I., Sultan, B., 2008b. What controls the isotopic composition of the African monsoon precipitation? Insights from event-based precipitation collected during the 2006 AMMA field campaign. Geophys. Res. Lett. 35, L24808.
Risi, C., Bony, S., Vimeux, F., Jouzel, J., 2010. Water-stable isotopes in the LMDZ4 general circulation model: model evaluation for present-day and past climates and applications to climatic interpretations of tropical isotopic records. J. Geophys. Res 115, D12118.
Rindsberger, M., Jaffe, S., Rahamim, S., Gat, J., 1990. Patterns of the isotopic composition of precipitation in time and space: data from the Israeli storm collection program. Tellus 42B, 263–271.
Rozanski, K., Araguas-Araguas, L., Gonfiantini, R., 1993. Isotopic patterns in modern global precipitation. In: Swart, P.K., Lohmann, K.C., McKenzie, J. (Eds.), Climate Change in Continental Isotopic Records. Geophysical Monograph, vol. 78. American Geophysical Union, Washington, DC, pp. 1–36.
Sachs, J., Sachse, D., Smittenberg, R., Zhang, Z., Battisti, D., Golubic, S., 2009. Southward movement of the Pacific intertropical convergence zone AD 1400–1850. Nat. Geosci. 2, 519–525.
Schmidt, G., LeGrande, A., Hoffman, 2007. Water isotope expressions of intrinsic and forced variability in a coupled ocean–atmosphere model. J. Geophys. Res. 112, D10103.
Stewart, M., 1975. Stable isotope fractionation due to evaporation and isotopic exchange of falling waterdrops: applications to atmospheric processes and evaporation of lakes. J. Geophys. Res 80 (9), 1133–1146.
Sturm, C., Vimeux, F., Krinner, G., 2007. Intraseasonal variability in South America recorded in stable water isotopes. J. Geophys. Res. 112, D20118.
Sturm, C., Zhang, Q., Noone, D., 2010. An introduction to stable water isotopes in climate models: benefits of forward proxy modeling for paleoclimatology. Clim. Past 6, 115–129.
Tian, L., Yao, T., MacClune, K., White, J., Schilla, A., Vaughn, B., Vachon, R., Ichiyanagi, K., 2007. Stable isotope variations in west China: a consideration of moisture sources. J. Geophys. Res. 112, D10112.
Tierney, J., Oppo, D., Rosenthal, Y., Russell, J., Linsley, B., 2010. Coordinated hydrological regimes in the Indo-Pacific region during the past two millennia. Paleoceanography 25, PA1102.
Tindall, J., Valdes, P., Sime, L., 2009. Stable water isotopes in HadCM3: Isotopic signature of El Niño Southern Oscillation and the tropical amount effect. J. Geophys. Res. Atmos. 114, D04111.
Treble, P.C., Chappell, J., Gagan, M.K., McKeegan, K.D., Harrison, T.M., 2005. In situ measurement of seasonal delta O-18 variations and analysis of isotopic trends in a modem speleothem from southwest Australia. Earth Planet. Sci. Lett. 233, 17–32.
Tremoy, G., Vimeux, F., Mayaki, S., Souley, I., Cattani, O., Risi, C., Favreau, G., Oi, M., 2012. A 1-year long $\delta^{18}O$ record of water vapor in Niamey (Niger) reveals insightful atmospheric processes at different timescales. Geophys. Res. Lett. 39, L08805.
Vimeux, F., Ginot, P., Schwikowski, M., Vuille, M., Hoffmann, G., Thompson, L.G., Schotterer, U., 2009. Climate variability during the last 1000 years inferred from Andean ice cores: a review of methodology and recent results. Palaeogeogr. Palaeoclimatol. Palaeoecol. 281, 229–241.
Vimeux, F., Tremoy, G., Risi, C., Gallaire, R., 2011. A strong control of the South American SeeSaw on the intra-seasonal variability of the isotopic composition of precipitation in the Bolivian Andes. Earth Planet. Sci. Lett 307, 47–58.
Vuille, M., Werner, M., Bradley, R.S., Keimig, F., 2005. Stable isotopes in precipitation in the Asian monsoon region. J. Geophys. Res. 110, D23108.
Wang, Y.J., Cheng, H., Edwards, R.L., An, Z.S., Wu, J.Y., Shen, C.C., Dorale, J.A., 2001. A high-resolution absolute-dated Late Pleistocene monsoon record from Hulu Cave, China. Science 294, 2345–2348.
Yamanaka, T., Shimada, J., Hamada, Y., Tanaka, T., Yang, Y.H., Zhang, W.J., Hu, C.S., 2004. Hydrogen and oxygen isotopes in precipitation in the northern part of the north china plain: climatology and interstorm variability. Hydrol. Processes 18 (12), 2211–2222.
Yuan, D.X., Cheng, H., Edwards, R.L., Dykoski, C.A., Kelly, M.J., Zhang, M.L., Qing, J.M., Lin, Y.S., Wang, Y.J., Wu, J.Y., Dorale, J.A., An, Z.S., Cai, Y.J., 2004. Timing, duration and transition of the last interglacial Asian Monsoon. Science 304, 575–578.
Zhang, C., 2005. Madden–Julian Oscillation. Rev. Geophys. 43, RG2003.